ChemBioChem

Research Article
doi.org/10.1002/cbic.202200209

Chemistry Europe
European Chemical Societies Publishing

www.chembiochem.org

A General Strategy for the Design and Evaluation of Heterobifunctional Tools: Applications to Protein Localization and Phase Separation

Rachel M. Lackner,[a] Will O'Connell,[b] Huaiying Zhang,*[c] and David M. Chenoweth*[a]

To mimic the levels of spatiotemporal control that exist in nature, tools for chemically induced dimerization (CID) are employed to manipulate protein-protein interactions. Although linker composition is known to influence speed and efficiency of heterobifunctional compounds, modeling or *in vitro* experiments are often insufficient to predict optimal linker structure. This can be attributed to the complexity of ternary complex formation and the overlapping factors that impact the effective concentration of probe within the cell, such as efflux and passive permeability. Herein, we synthesize a library of modular chemical tools with varying linker structures and perform quantitative microscopy in live cells to visualize dimerization in real-time. We use our optimized probe to demonstrate our ability to recruit a protein of interest (POI) to the mitochondria, cell membrane, and nucleus. Finally, we induce and monitor local and global phase separation. We highlight the importance of quantitative approaches to linker optimization for dynamic systems and introduce new, synthetically accessible tools for the rapid control of protein localization.

Introduction

Chemically induced dimerization (CID) is a powerful tool for the study of complex cellular processes, such as cell growth, death, division, and signaling, that are tightly regulated by protein-protein interactions (PPIs) with high levels of spatiotemporal control.[1] Probes for CID typically consist of small, heterobifunctional molecules that are designed to localize a protein of interest (POI) proximal to a second POI, a subcellular compartment, or to reconstitute a single split protein construct. Chemical probes for the control of PPIs benefit from increased levels of spatiotemporal control relative to traditional genetic techniques, such as knockdown or mutagenesis.

Our group has previously developed a modular system that can be used for CID.[2] This system makes use of the specific binding between *E. Coli* dihydrofolate reductase (eDHFR) and the antibiotic trimethoprim (TMP),[3] and between HaloTag protein and a chlorohexane moiety.[4] Upon entry into the cell, the HaloTag protein covalently and irreversibly binds to the chloroalkane through nucleophilic attack and displacement of chlorine, followed by noncovalent, reversible binding of TMP to eDHFR.

Although proteolysis targeting chimeras (PROTACs) are among the most well-known examples of heterobifunctional tools for CID, the interest in systems that can induce biological events via PPIs has exploded in recent years.[5] In addition to PROTACs, heterobifunctional, or "chimeric," small molecules for the control of deubiquitination,[6] phosphorylation,[7] glycosylation,[8] lysosomal degradation,[9] and autophagy[10] have been reported. Despite differences in their downstream effects, these tools also operate via the control of protein proximity, resulting in the formation of a ternary complex between bifunctional molecule and its targets and the subsequent increase in the effective molarity of the PPI. Therefore, despite serving different aims and targeting different systems, these tools require similar considerations.[11] It has been well-documented, particularly in the PROTAC literature, that the length and composition of the linker of a multicomponent probe has significant impact on its efficiency, speed, and, in some cases, even its target.[12] The importance of linker optimization, or "linkerology," is not limited to PROTACs, or even bifunctional compounds more generally,[13] and must also be considered in the development of stapled peptides,[14] inhibitors,[15] and prodrugs.[16] Although protein docking can aid in the selection of an optimal linker based on steric considerations, other factors, such as positive or negative cooperativity, efflux, cell permeability, and protein microenvironment are less easily predicted and can complicate dimerization *in cellulo*. Previously, a protein translocation-based imaging assay in live cells was combined with Western blot analysis to optimize the linker length of plasma membrane-targeting bifunctional probes, but to the best of our knowledge, there has yet to be an example of a real-time, quantitative comparison of bifunctional tools for the control of protein

[a] R. M. Lackner, Dr. D. M. Chenoweth
Department of Chemistry
School of Arts and Sciences, University of Pennsylvania
Philadelphia, Pennsylvania 19104 (USA)
E-mail: dcheno@sas.upenn.edu
[b] W. O'Connell
Department of Chemical Engineering
Carnegie Mellon University, Pittsburgh, PA 15213 (USA)
[c] Dr. H. Zhang
Department of Biological Sciences
Mellon College of Science, Carnegie Mellon University
Pittsburgh, PA 15213 (USA)
E-mail: huaiyinz@andrew.cmu.edu

Supporting information for this article is available on the WWW under https://doi.org/10.1002/cbic.202200209

localization in live cells.[13c] Therefore, it is imperative to employ a high-throughput, quantitative, cell-based approach to facilitate the rational design of probes that can be used to monitor and control complex processes in live cells.

Although the TMP-Halo system has been used to manipulate complex cellular processes such as organelle transport,[17] mitosis,[2b,c, 18] meiosis,[19] cell-cell adhesion,[20] translational activation,[21] and phase separation,[22] there has yet to be a targeted exploration of the impact of linkers on dimerization in the TMP-Halo system, in part due to the complexities of ternary complex formation and the difficulty of assessing the cross-linking of the TMP-Halo probe via *in vitro* methods, due to the reversible nature of the TMP-eDHFR interaction. Therefore, the first- and second-generation TMP-Halo probes, **TH** (Figure 1a) and **TNH** (Figure 1b), were developed without a significant focus on linker optimization.

To explore the effect of linker length and composition on CID within the TMP-Halo system, we took advantage of its modular nature to synthesize a library of TMP-Halo probes with varying linker structures. We developed a real-time, microscopy-based assay to evaluate each probe in a quantitative, reproducible, and scalable manner. We then evaluated each probe's ability to recruit a POI to the mitochondria in live cells, demonstrating that minor changes to the linker can dramatically impact dimerization. Based on these studies, we identified a top-performing linker, which was used to localize a POI to the cell membrane and nucleus. Finally, we demonstrated the utility of our optimized tool for the manipulation of dynamic cellular processes such as local and global phase separation. The purpose of this study is not to serve as a comprehensive exploration of chemical space or to definitively disentangle the myriad effects that impact dimerization speeds, but to demonstrate the complex considerations that must be made when choosing a probe for CID and to highlight the utility of a single microscopy-based readout for the evaluation and comparison of heterobifunctional probes in live cells.

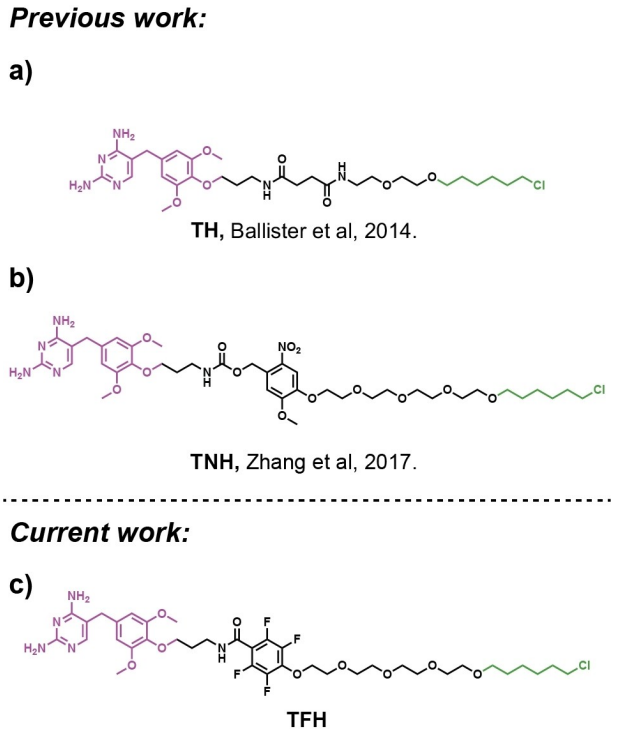

Figure 1. First, second, and third generation TMP-Halo probes for chemically induced dimerization. Trimethoprim (TMP) highlighted in purple and HaloTag ligand highlighted in green.

Results and Discussion

The first objective for improving the design of our probe was to explore the effect of linker length on dimerization speed. The synthesis of our first generation TMP-Halo dimerizer, **TH** (Figure 1a) requires six steps, making it an impractical route to generate a library of probes of different lengths.[2a] Since polyethylene glycol (PEG) is a hydrophilic, flexible linker that is commercially available in multiple lengths, we were intrigued by the possibility of exploring various PEG-based linkers as a starting point to optimize dimerization speed and efficiency. We synthesized a series of five PEG-based TMP-Halo derivatives, each in four steps starting from trimethoprim, with linker lengths of 4, 5, 6, 8, and 10 PEG units (Figure 2a). To observe dimerization over time, we developed a quantitative assay that allows us to observe recruitment of freely diffusing protein to a fixed position in live cells via a microscopy-based readout. HeLa cells stably expressing 1) mCherry fused to eDHFR and 2) HaloTag enzyme fused to both GFP and the *Listeria monocytogenes* ActA protein were used, as the mitochondria are static cellular features that we can easily monitor over time. In the absence of dimerizer, mCherry-eDHFR is diffusively localized through the cytosol of the cell, whereas GFP-Halo-ActA is localized at the cytosolic face of the mitochondria. Following probe treatment, dimerization can be visualized as the colocalization of mCherry and GFP increases over time.

Dimerization of **4TH** was too slow to be visualized, even when monitored over 5 hours (Figure S1), presumably due to the short distance between TMP and HaloTag causing negative steric hindrance and limiting interaction with eDHFR. Cells treated with **5TH** also exhibited slow dimerization, though low levels of colocalization could be visualized after approximately 60 minutes of incubation, indicating that the addition of even a single PEG unit can considerably increase dimerization speeds (Figure 2c). Due to the modest increase in signal resulting from dimerization relative to the decrease in signal caused by photobleaching, dimerization of **4TH** and **5TH** was not quantified. In contrast, treatment of cells with **6TH** showed a considerable increase in dimerization speed ($t_{1/2}$ ~25 minutes) (Figure 2b,c). It is evident from these findings that a minimum linker length is necessary for speed and efficiency of dimerization. It is worth noting that a version of **5TH** in which TMP is blocked with a photocleavable protecting group (PPG) has been shown to promote rapid dimerization following photocleavage in a similar system.[23] The use of a PPG allows cells to be pre-saturated with higher concentrations of probe and dimerization to be initiated only after HaloTag sites are occupied, essentially transforming the reaction into a binary

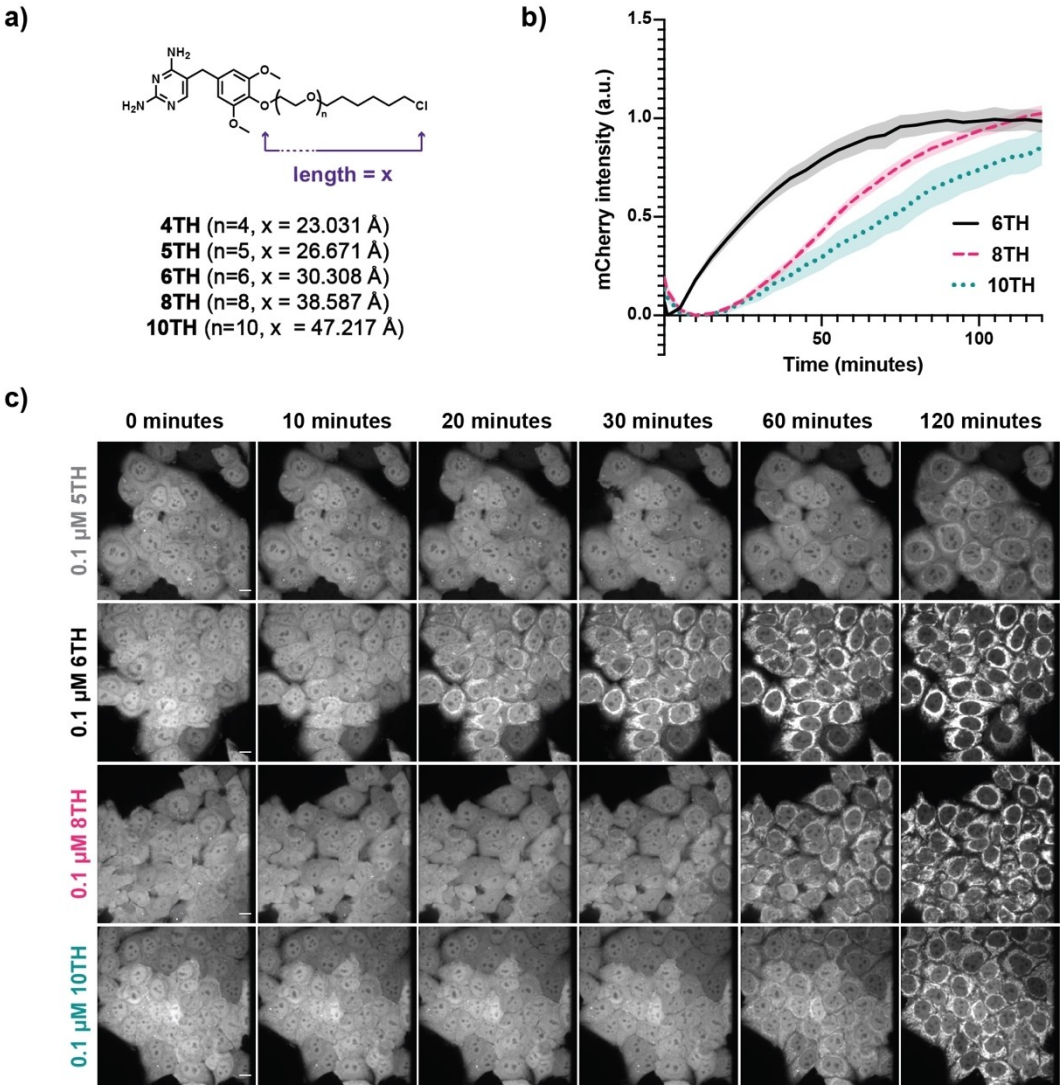

Figure 2. Comparison of PEG-based linkers. a) Lengths of probes (dihedral angles set to 180°) were measured from the *para* oxygen of TMP to the chlorine of HaloTag ligand. HeLa cells expressing mCherry-eDHFR and GFP-HaloTag-ActA were treated with probe and imaged every 5 minutes for 2 hours. b) mCherry intensity at the mitochondria was quantified over time. Error bars represent SEM (n = 9 fields of view, multiple cells per field, from 3 independent experiments). c) Over time, mCherry intensity at the mitochondria increases while cytosolic levels decrease. Scale bar, 10 µm.

(rather than ternary) complexation with a high effective concentration of probe. Therefore, a dimerizer that works well when protected with a PPG is not necessarily ideal in the absence of a PPG, further emphasizing the need for a rigorous, quantitative approach for linker selection.

We then moved on to **8TH** and **10TH**. Both compounds facilitated dimerization more slowly than **6TH**, with **8TH** reaching 50% maximum colocalization in approximately 55 minutes and **10TH** requiring closer to 70 minutes to achieve the same effect (Figure 2b,c). From this experiment, it was not clear if slower dimerization could be explained by the increased entropy of the longer linkers making formation of the ternary complex less likely,[24] or if the longer linker lengths were less able to permeate cells due to a combination of their large size (MW = 658, 747, and 835 for **6TH**, **8TH**, and **10TH**, respectively) and the increased hydrophilicity of additional PEG units.

We were interested in exploring the source of these differences between **6TH** and the longer linkers in order to highlight the complexity of overlapping factors that control dimerization and demonstrate the benefits of a single, real-time readout over multiple *in vitro* experiments.

We incubated cells with verapamil, a small molecule efflux inhibitor, prior to treatment with probe.[25] Although the rate of dimerization with **6TH** remained mostly unchanged, **8TH** and **10TH** showed faster dimerization in the presence of verapamil than in untreated cells (Figure S2). This suggests that efflux contributes to slower dimerization of **8TH** and **10TH** under normal conditions. In fact, after pretreatment with verapamil, both **8TH** and **10TH** showed higher maximum mCherry intensity at the mitochondria after two hours of imaging than **6TH**. Intriguingly, in the presence of verapamil, cells treated with **8TH** underwent faster dimerization than those treated

with **10TH**. This can be explained by the additional PEG units and larger size of **10TH** causing a decrease in passive permeability, and we propose that the effects of efflux and passive permeability are cumulative and complex. We suggest that longer linkers may therefore represent a compromise between improved sterics and reduced equilibrium concentration of probe due to the overlapping effects of permeability and efflux.

With this in mind, we hypothesize that although **8TH** and **10TH** are long enough to overcome the negative steric clash between the eDHFR and HaloTag proteins, the longer linker lengths cause a lower concentration of probe within the cell at equilibrium, resulting in decreased speeds of dimerization. We conclude that linker length is a critical factor in dimerization efficiency and that a length of at least 27–30 angstroms is necessary for dimerization. Longer lengths up to 38 angstroms might lead to an increase in dimerization speed, but one must also consider the cost of reduced permeability and efflux.

Having confirmed that optimization of linker length is critical for efficient dimerization with the TMP-Halo system, we were interested in further improving the speed of dimerization. Aromatic rings can confer additional rigidity and lipophilicity to a probe, which can improve permeability or stabilize formation of the ternary complex. Therefore, the introduction of an aromatic ring is another strategy to improve our probe's physicochemical properties.

We synthesized two TMP-Halo probes to explore how the addition of an aromatic ring into the linker could facilitate dimerization. Addition of aromatic fluorines is known to further increase lipophilicity and passive permeability across the cell membrane without increasing molecular volume and has been demonstrated to improve the activity of probes for CID that combine HaloTag with the covalent SNAP-Tag system.[13a,26] We therefore synthesized an unsubstituted (**T**MP-**B**enzamide-**H**alo, **TBH**) and a tetrafluorinated (**T**MP-**F**luorobenzamide-**H**alo, **TFH**) version of our aromatic TMP-Halo probes (Figure 3a-b). Although **TBH** and **TFH** involve slightly lengthier syntheses than the PEG-based linkers (see Supporting Information), they are nonetheless simpler than our current fastest dimerizer, **TNH** (Figure 1b), which is synthesized in 10 steps and must be kept away from ambient light following introduction of the light-sensitive nitroveratryl group.[2b]

With **TBH**, we observed rapid dimerization ($t_{1/2}$ ~14 minutes), with significant improvement compared to the all-PEG linkers (Figure 3a). **TFH** showed even more dramatic improvement ($t_{1/2}$ ~7 minutes) (Figure 3b). This can be explained by the increased lipophilicity of **TFH** due to the addition of aromatic fluorines. Both probes were tested at three concentrations (0.01 μM, 0.1 μM, and 1.0 μM). We were intrigued to observe that **TFH** at 0.1 μM and 1.0 μM concentration enter cells at a similar rate before a plateauing of signal at the higher concentration after approximately 8 minutes. This difference suggests that **TFH** may be taken up by cells so quickly that even relatively low concentrations result in a high local concentration leading to rapid dimerization. In contrast, upon treatment with 1.0 μM **TBH**, mCherry intensity continued to slowly increase over time rather than reaching a stable level.

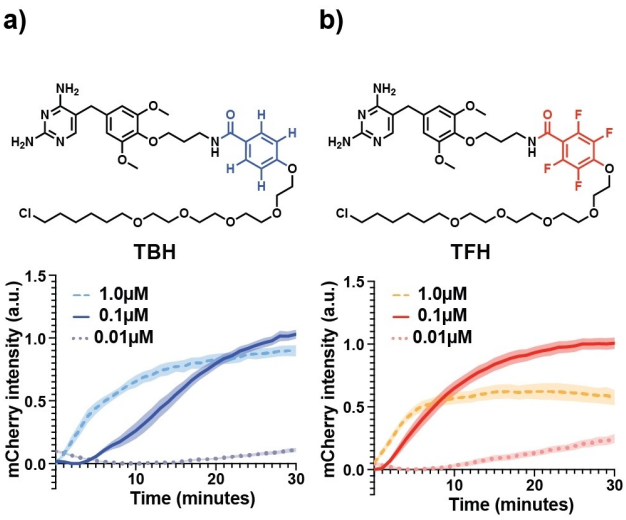

Figure 3. Chemical structure and concentration-dependent dimerization of a) **TBH** and b) **TFH**. Error bars represent SEM (n = 9 fields of view from 3 independent experiments, greater than 10 cells per field).

Although TMP exhibits tight, specific binding to eDHFR (K_i = 0.08 nM),[27] free TMP can be used to reverse dimerization within minutes.[2a] The reversibility of TMP-eDHFR binding might explain the continued increase of signal even at higher concentrations of **TBH**, whereas the equilibrium of **TFH** may favor the bound state due to non-specific secondary interactions with protein, keeping the on/off rate low. Replacement of C–H bonds with C–F bonds is also known to lead to increased levels of aggregation in aqueous systems,[28] possibly contributing to the increased "stickiness" of **TFH** molecules with each other and reducing the capacity for binding at higher concentrations of probe. Given the complex balance between cellular uptake, protein binding equilibria, and possible linker aggregation effects, we cannot attribute these effects to a single physiochemical phenomenon without further study, but it is clear that a simple modification, such as fluorination of an aromatic linker, has profound implications for dimerization speed.

Having optimized our TMP-Halo system, we were interested in applying our new dimerizer to the recruitment of proteins to subcellular locations beyond the mitochondria. We first tried recruitment to the plasma membrane, as the plasma membrane is densely populated with proteins that are implicated in cell signaling, cell-cell fusion, immune response, endocytosis, and exocytosis,[29] and is therefore a desirable location for rapid control of PPIs. HeLa cells were transfected to express cytosolic mCherry-eDHFR and a fusion protein containing GFP, Haloenzyme, and a CAAX motif for membrane targeting.[30] We observed localization at the membrane as well as disappearance of mCherry signal at the nucleus and cytosol over the course of two hours, indicating that dimerization had taken place (Figure S3a). We then focused on directing protein localization to the chromatin, as the movement of proteins to and from the chromatin is integral for nuclear functions such as transcription.[31] We once again transiently transfected cytosolic

mCherry-eDHFR into HeLa cells, this time targeting the nucleus by co-expressing a fusion of GFP, Haloenzyme, and Histone H2B, which allowed us to visualize the nucleus of the cell[32] and recruit mCherry-eDHFR to the nucleus upon treatment with **TFH** (Figure S3b). These proof-of-concept experiments further demonstrate the potential of **TFH** as a universal tool for manipulating biological processes at the cellular level via the localization of cytosolic proteins with temporal control.

Having shown that **TFH** can direct proteins to various critical subcellular locations, we were curious to apply our probe to the manipulation of complex, dynamic processes that necessitate rapid dimerization. Liquid-liquid phase separation, in which biomolecules such as proteins and nucleic acids form condensed liquid-like phases called condensates, has emerged as a critical mechanism by which cells self-organize.[33] This process has been implicated in the control of gene expression,[34] signal transduction,[35] stress response,[36] neurodegenerative diseases such as amyotrophic lateral sclerosis (ALS),[37] and cancer.[22,38] However, the precise function and molecular-level mechanism of liquid-liquid phase separation in cells is still poorly understood, despite a growing body of research into its relevance. The absence of information regarding the spatiotemporal regulation of phase separation and relative lack of tools for probing this process in living cells makes it an ideal application for CID.[33b] Optogenetic techniques have been developed, but these require continual irradiation with high energy blue light, limiting their application to relatively brief experiments due to the potential for photobleaching and tissue damage.[39]

We first demonstrated the ability of **TFH** to control condensate formation on chromatin, as phase separation has been implicated in many chromatin functions, such as protein enrichment and structural organization.[40] We aimed to induce condensates on telomeres (repetitive DNA sequences at chromosome ends) via the dimerization of a telomere-binding protein, TRF1, and the arginine/glycine-rich (RGG) domain of LAF-1, a disordered protein found in P granules that is known to form liquid condensates (Figure 4a).[22,41] Within 10 minutes after adding **TFH**, RGG foci that were colocalized with TRF1 appeared (Figure 4d). RGG foci also became brighter and rounder over time and coalesced with each other, indicating the formation of phase separated liquid droplets on telomeres (Figure 4d–g). RGG recruitment also led to an increase in TRF1 intensity (Figure 4e). This is because RGG droplet fusion causes telomeres to cluster, and RGG condensation recruits RGG-dimerized TRF1 to the telomeres, enriching TRF1 beyond the TRF1 that was bound directly to telomeric DNA (Figure 4a). Neither increase in TRF1 intensity nor telomere clustering were observed when recruiting mCherry-eDHFR alone (Figure 4c, S4). Instead, TRF1 intensity decreased over time in mCherry-eDHFR cells, likely due to photobleaching, as a similar decrease was observed in cells expressing mCherry-eDHFR that were not treated with **TFH** (Figure 4b). Furthermore, we demonstrated the reversibility of phase separation through the addition of free TMP, with full reversal of binding accomplished within an hour (Supplementary Video 1, Figure S4).

To minimize the effects of photobleaching and assess RGG phase separation and RGG-induced telomere clustering more accurately, we incubated cells with **TFH** for 5 hours and fixed them for imaging. Similar to what was observed with live imaging and consistent with RGG-induced phase separation, TRF1 foci decreased in quantity, grew in volume, and became brighter after recruiting RGG-mCherry-RGG-eDHFR but not after recruiting mCherry-eDHFR (Figure S5). Interestingly, after recruiting mCherry-eDHFR, TRF1 foci still decreased in quantity and became smaller and dimmer, even when light exposure had been greatly minimized, indicating that factors other than photobleaching play a role. One possible explanation is that mCherry underwent fluorescence quenching as the concentration increased at the telomeres after recruitment.[42] Nevertheless, these results show that **TFH** is a desirable choice of tool for inducing condensates on sub-cellular structures.

We next used **TFH** to induce global phase separation in the nucleoplasm/cytoplasm, which is desirable for many applications, as a large number of condensates, such as stress granules and promyelocytic leukemia (PML) bodies, are not localized to any subcellular structures. To do so, we fused 3 copies of HaloTag protein to a synthetic hexamer, HoTag3, to generate a 18mer seed that will promote droplet formation after dimerizing to the phase separation protein (Figure 5a).[43] We first tried to recruit RGG to the 18mer seed and interestingly did not see any condensate formation in the nucleus at protein levels similar to that used for condensate formation on telomeres. This indicates that the less mobile and highly repetitive telomeres are more efficient at seeding condensates.

We then decided to induce phase separation using the C-terminus disordered region of hnRNPA1 (termed as hnRNPA1 C), which has previously been shown to phase separate in the nucleoplasm.[39a] hnRNPA1 C is concentrated in the nucleus, and in some cells, we observed condensates that formed before addition of **TFH**. Interestingly, RGG shows a more diffusive patten at similar protein levels, suggesting that hnRNPA1 C is more prone to phase separation than RGG. Supporting this notion, addition of **TFH** to hnRNPA1 C cells led to colocalization of HOTag3 with pre-existing hnRNPA1 C droplets and caused them to grow brighter and bigger over time (Figure 5b–c). In addition, new hnRPA1 C condensates nucleated in the cytoplasm where hnRNPA1 C was at a low concentration (Figure 5b). The newly formed cytoplasmic condensates coarsened over time and eventually became much bigger than those in the nucleus. This result is in agreement with a recent report that droplet growth in the nucleus is inhibited by chromatin.[39e]

These examples illustrate the ability of **TFH** to induce both local phase separation on subcellular structures and global phase separation in the nucleoplasm/cytoplasm and to fulfil an existing need for rapid control of phase separation without the use of damaging, high energy light. In addition, the fact that **TFH** lacks the light sensitivity of **TNH** and can be synthesized in three fewer steps[2b] makes it a clear choice for control and observation of dynamic biological processes including, but not limited to, phase separation.

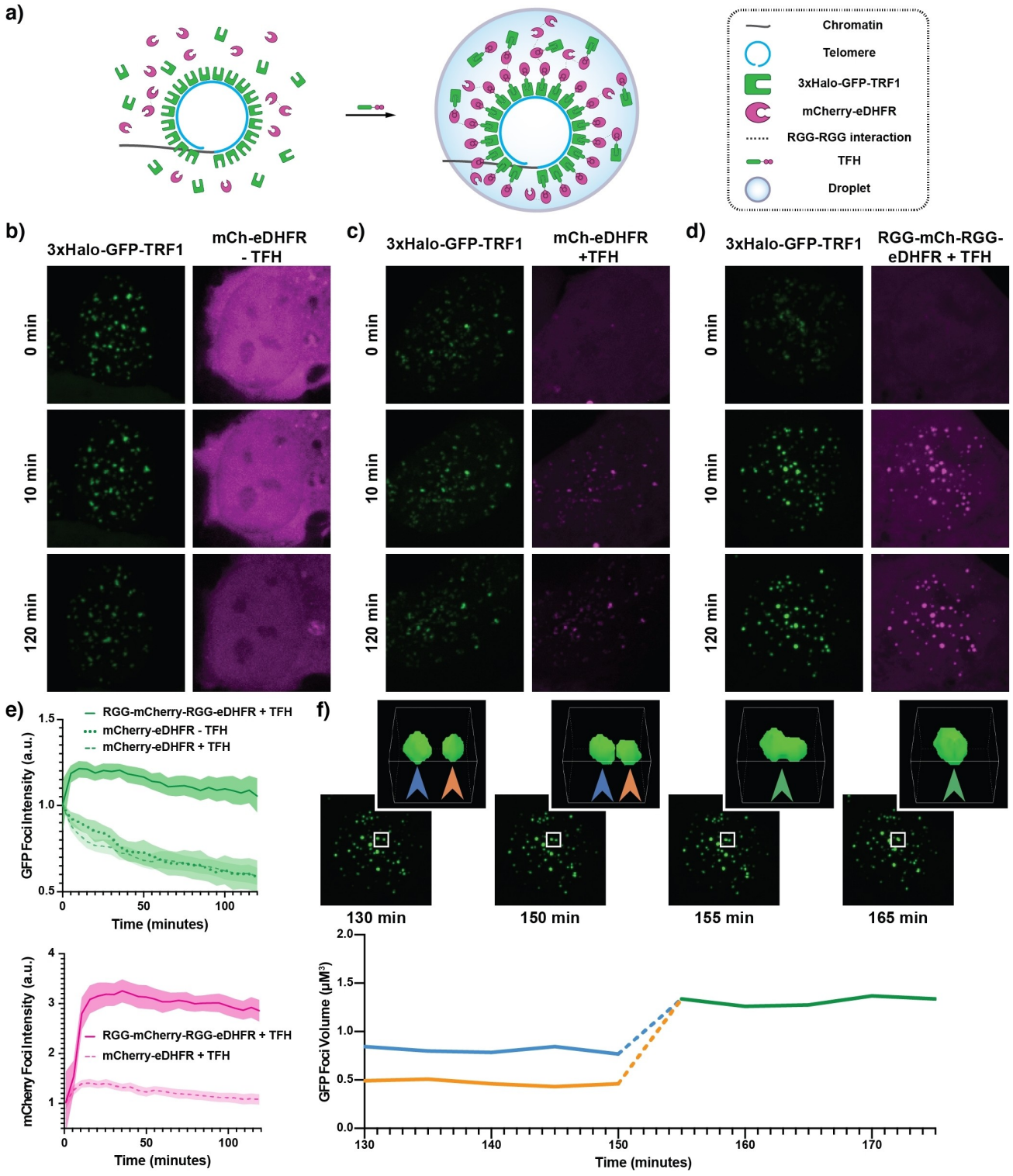

Figure 4. TFH dimerization induced protein phase separation on telomeres. a) Schematic for induction of droplet formation on telomeres. When RGG and TRF1 are dimerized by **TFH**, the concentration of RGG at the telomeres is increased above the threshold for phase separation, resulting in RGG condensation on the telomeres. RGG condensation leads to further TRF1 enrichment without directly binding to telomere DNA. b–d) Snapshots of U-2OS cells after dimerizing RGG to TRF1. mCherry-eDHFR is used as a control for recruiting non-phase separating proteins, and mCherry-eDHFR without **TFH** is used as a control for photobleaching. Scale bar = 5 μm. e) GFP and mCherry foci intensities over time. Foci intensities are total intensity per foci averaged among all foci in one cell and are scaled such that initial values are unity where foci are present – elsewise not shown. Error bars represent 95% confidence interval. N = 61 cells from 5 experiments. f) GFP foci coalescence after recruiting RGG-mCherry-RGG-eDHFR. Arrows denote two foci which begin to coalesce into one starting at 155 min. Inset represents 3-D binary determined by image processing.

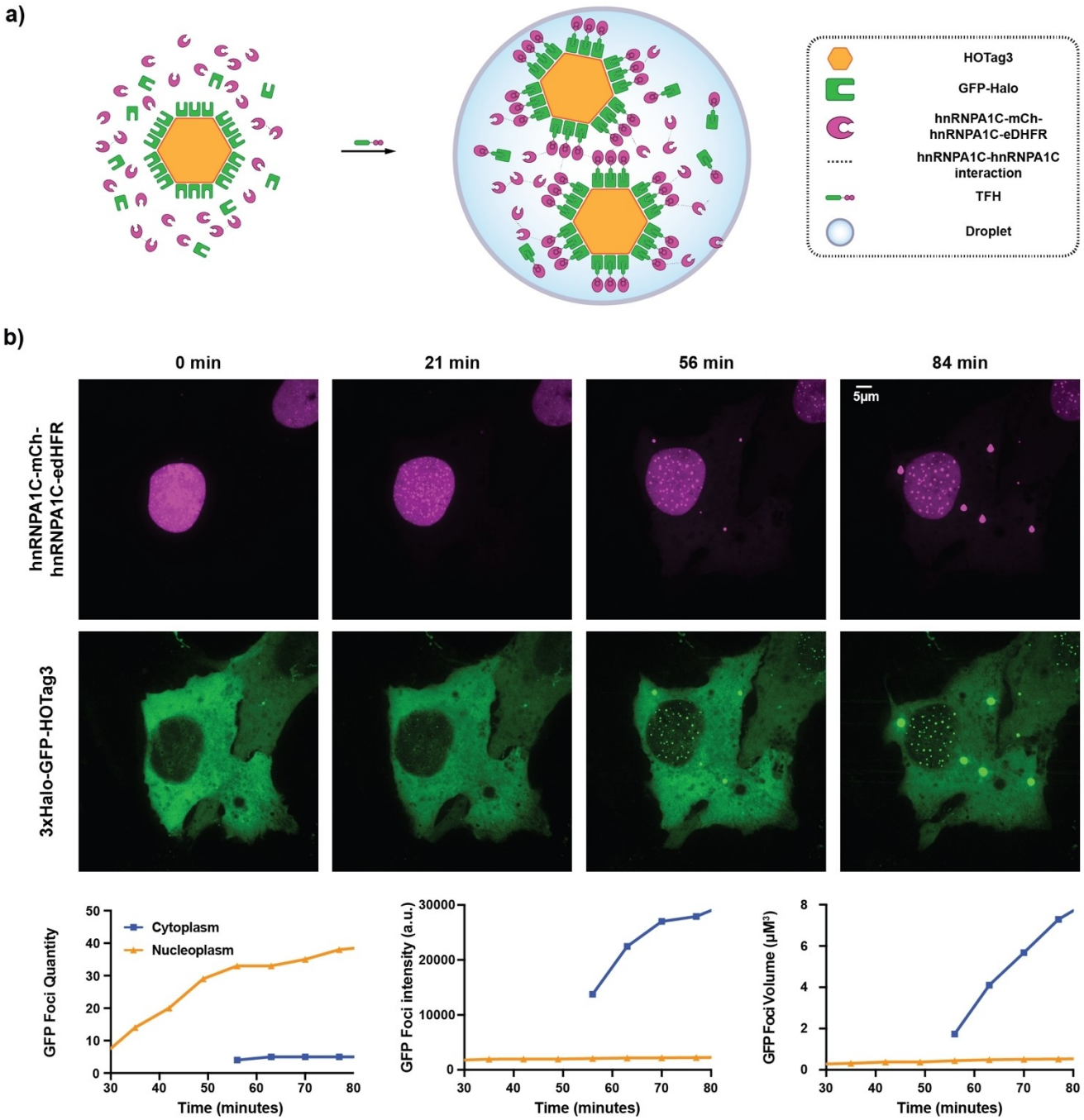

Figure 5. TFH dimerization induced phase separation in the nucleoplasm and cytoplasm with oligomer seeds. a) Schematics to induce phase separation with the hexameric HOTag3, which offers 18 Halo sites to dimerize hnRNPA1C-mCherry-hnRNPA1C-eDHFR in order to increase local concentration of C-terminus IDR of hnRNPA1 (hnRNPA1C) and induce phase separation. b) Snapshots of U-2 OS cells with **TFH**-induced hnRNPA1 droplets in the nucleus and cytoplasm and quantification of average GFP foci number, volume, and intensity over time in the nucleus and cytoplasm within the above cells, following addition of **TFH**.

Conclusion

We have developed a general approach to quantitatively investigate the effects of linker structure in live cells and applied this method to the rational design of heterobifunctional probes based on the TMP-Halo system. Our results emphasize the impact of linker structure on speed of dimerization and highlight the myriad of variables (such as efflux, permeability, and sterics) that are necessary to consider when synthesizing and testing probes for CID. Attempts to assess each factor independently can be time consuming and potentially misleading, and we have demonstrated that the optimization of one factor, such as sterics, can lead to reduction of another, such as cell entry. In contrast, our approach enables us to utilize a

single, real-time assay to evaluate the additive effects of these variables in a holistic manner. In context with observations that have been made in the peptide stapling field, the PROTAC field, and other medicinal chemistry efforts where linker composition influences binding kinetics, these results emphasize that the choice of linker has profound effects and should be considered as carefully as one considers the choice of protein/ligand pair. It is therefore necessary to develop methods by which both covalent and noncovalent tools can be rigorously evaluated and compared. We find that although there is a minimum length for the TMP-Halo probe, longer linkers are not necessarily ideal, due to a combination of entropy and lower rates of cell entry resulting from a combination of efflux and suboptimal permeability. We developed new, non-cleavable dimerizers that contain aromatic rings and lipophilic moieties for improving cellular uptake, demonstrating that the introduction of a fluorinated ring results in faster dimerization with high temporal control. Finally, we highlighted several applications of the optimized dimerizer, demonstrating that it can control protein transport to multiple cellular organelles and rapidly initiate local and global phase separation. Our general approach can be modified to evaluate other heterobifunctional systems for CID and compare existing tools with each other in a quantitative, high-throughput manner. We also expect that the resulting probes can be used in combination with existing chemigenetic tools to answer pressing questions in biology via the manipulation of protein localization with high levels of control.

Acknowledgements

The authors would like to thank Dr. Daniel Wu for helpful discussions early in the project. This work was supported by funding from the University of Pennsylvania (D.M.C.), National Institutes of Health (Grant NIH R01-GM118510 to D.M.C.), and National Science Foundation Faculty Early Career Development Program (NSF CAREER no. 2145083 to H.Z.). The NIH supplemental awards 3R01GM118510-03S1 and 3R01GM087605-06S1, as well as the Vagelos Institute for Energy Science and Technology, supported the purchase of the NMR instruments used in this study.

Conflict of Interest

The authors declare no conflict of interest.

Data Availability Statement

The data that support the findings of this study are available from the corresponding author upon reasonable request.

Keywords: bioorganic chemistry · chemically induced dimerization · heterobifunctional · protein-protein interactions · phase separation

[1] B. Z. Stanton, E. J. Chory, G. R. Crabtree, *Science* **2018**, *359*, eaao5902.
[2] a) E. R. Ballister, C. Aonbangkhen, A. M. Mayo, M. A. Lampson, D. M. Chenoweth, *Nat. Commun.* **2014**, *5*, 5475; b) H. Zhang, C. Aonbangkhen, E. V. Tarasovetc, E. R. Ballister, D. M. Chenoweth, M. A. Lampson, *Nat. Chem. Biol.* **2017**, *13*, 1096–1101; c) C. Aonbangkhen, H. Zhang, D. Z. Wu, M. A. Lampson, D. M. Chenoweth, *J. Am. Chem. Soc.* **2018**, *140*, 11926–11930.
[3] L. W. Miller, Y. Cai, M. P. Sheetz, V. W. Cornish, *Nat. Methods* **2005**, *2*, 255–257.
[4] G. V. Los, L. P. Encell, M. G. McDougall, D. D. Hartzell, N. Karassina, C. Zimprich, M. G. Wood, R. Learish, R. F. Ohana, M. Urh, D. Simpson, J. Mendez, K. Zimmerman, P. Otto, G. Vidugiris, J. Zhu, A. Darzins, D. H. Klaubert, R. F. Bulleit, K. V. Wood, *ACS Chem. Biol.* **2008**, *3*, 373–382.
[5] A. E. Modell, S. Lai, T. M. Nguyen, A. Choudhary, *Cell Chem. Biol.* **2021**, *28*, 1081–1089.
[6] N. J. Henning, L. Boike, J. N. Spradlin, C. C. Ward, G. Liu, E. Zhang, B. P. Belcher, S. M. Brittain, M. J. Hesse, D. Dovala, L. M. McGregor, R. Valdez Misiolek, L. W. Plasschaert, D. J. Rowlands, F. Wang, A. O. Frank, D. Fuller, A. R. Estes, K. L. Randal, A. Panidapu, J. M. McKenna, J. A. Tallarico, M. Schirle, D. K. Nomura, *Nat. Chem. Biol.* **2022**, *18*, 412–421.
[7] a) S. U. Siriwardena, D. N. P. Munkanatta Godage, V. M. Shoba, S. Lai, M. Shi, P. Wu, S. K. Chaudhary, S. L. Schreiber, A. Choudhary, *J. Am. Chem. Soc.* **2020**, *142*, 14052–14057; b) S. Yamazoe, J. Tom, Y. Fu, W. Wu, L. Zeng, C. Sun, Q. Liu, J. Lin, K. Lin, W. J. Fairbrother, S. T. Staben, *J. Med. Chem.* **2020**, *63*, 2807–2813; c) P.-H. Chen, Z. Hu, E. An, I. Okeke, S. Zheng, X. Luo, A. Gong, S. Jaime-Figueroa, C. M. Crews, *ACS Chem. Biol.* **2021**, *16*, 2808–2815.
[8] a) D. H. Ramirez, C. Aonbangkhen, H.-Y. Wu, J. A. Naftaly, S. Tang, T. R. O'Meara, C. M. Woo, *ACS Chem. Biol.* **2020**, *15*, 1059–1066; b) Y. Ge, D. H. Ramirez, B. Yang, A. K. D'Souza, C. Aonbangkhen, S. Wong, C. M. Woo, *Nat. Chem. Biol.* **2021**, *17*, 593–600.
[9] a) G. Ahn, S. M. Banik, C. L. Miller, N. M. Riley, J. R. Cochran, C. R. Bertozzi, *Nat. Chem. Biol.* **2021**, *17*, 937–946; b) S. M. Banik, K. Pedram, S. Wisnovsky, G. Ahn, N. M. Riley, C. R. Bertozzi, *Nature* **2020**, *584*, 291–297.
[10] a) Z. Li, C. Zhu, Y. Ding, Y. Fei, B. Lu, *Autophagy* **2020**, *16*, 185–187; b) D. Takahashi, J. Moriyama, T. Nakamura, E. Miki, E. Takahashi, A. Sato, T. Akaike, K. Itto-Nakama, H. Arimoto, *Mol. Cell* **2019**, *76*, 797–810.e710.
[11] C. J. Gerry, S. L. Schreiber, *Nat. Chem. Biol.* **2020**, *16*, 369–378.
[12] a) D. L. Buckley, K. Raina, N. Darricarrere, J. Hines, J. L. Gustafson, I. E. Smith, A. H. Miah, J. D. Harling, C. M. Crews, *ACS Chem. Biol.* **2015**, *10*, 1831–1837; b) K. Cyrus, M. Wehenkel, E.-Y. Choi, H.-J. Han, H. Lee, H. Swanson, K.-B. Kim, *Mol. BioSyst.* **2011**, *7*, 359–364; c) G. M. Burslem, B. E. Smith, A. C. Lai, S. Jaime-Figueroa, D. C. McQuaid, D. P. Bondeson, M. Toure, H. Dong, Y. Qian, J. Wang, A. P. Crew, J. Hines, C. M. Crews, *Cell Chem. Biol.* **2018**, *25*, 67–77.e63; d) A. Zorba, C. Nguyen, Y. Xu, J. Starr, K. Borzilleri, J. Smith, H. Zhu, K. A. Farley, W. Ding, J. Schiemer, X. Feng, J. S. Chang, D. P. Uccello, J. A. Young, C. N. Garcia-Irrizary, L. Czabaniuk, B. Schuff, R. Oliver, J. Montgomery, M. M. Hayward, J. Coe, J. Chen, M. Niosi, S. Luthra, J. C. Shah, A. El-Kattan, X. Qiu, G. M. West, M. C. Noe, V. Shanmugasundaram, A. M. Gilbert, M. F. Brown, M. F. Calabrese, *Proc. Natl. Acad. Sci. USA* **2018**, *115*, E7285-E7292.
[13] a) D. Erhart, M. Zimmermann, O. Jacques, Matthias B. Wittwer, B. Ernst, E. Constable, M. Zvelebil, F. Beaufils, Matthias P. Wymann, *Chem. Biol.* **2013**, *20*, 549–557; b) L. Zhou, C. Fang, P. Wei, S. Liu, Y. Liu, L. Lai, *J. Med. Chem.* **2008**, *51*, 3360–3366; c) A. Nakamura, C. Oki, K. Kato, S. Fujinuma, G. Maryu, K. Kuwata, T. Yoshii, M. Matsuda, K. Aoki, S. Tsukiji, *ACS Chem. Biol.* **2020**, *15*, 1004–1015.
[14] Y. S. Tan, D. P. Lane, C. S. Verma, *Drug Discovery Today* **2016**, *21*, 1642–1653.
[15] A. A. Reinke, J. E. Gestwicki, *Chem. Biol. Drug Des.* **2007**, *70*, 206–215.
[16] Y. Ikuta, Y. Koseki, T. Onodera, H. Oikawa, H. Kasai, *Chem. Commun.* **2015**, *51*, 12835–12838.
[17] a) E. R. Ballister, S. Ayloo, D. M. Chenoweth, M. A. Lampson, E. L. F. Holzbaur, *Curr. Biol.* **2015**, *25*, R407-R408; b) X. Chen, M. Venkatachalapathy, L. Dehmelt, Y.-W. Wu, *Angew. Chem. Int. Ed.* **2018**, *57*, 11993–11997; *Angew. Chem.* **2018**, *130*, 12169–12173.
[18] G.-Y. Chen, F. Renda, H. Zhang, A. Gokden, D. Z. Wu, D. M. Chenoweth, A. Khodjakov, M. A. Lampson, *J. Cell Biol.* **2021**, *220*, e202007030.
[19] T. Akera, L. Chmátal, E. Trimm, K. Yang, C. Aonbangkhen, D. M. Chenoweth, C. Janke, R. M. Schultz, M. A. Lampson, *Science* **2017**, *358*, 668.
[20] D. Ollech, T. Pflästerer, A. Shellard, C. Zambarda, J. P. Spatz, P. Marcq, R. Mayor, R. Wombacher, E. A. Cavalcanti-Adam, *Nat. Commun.* **2020**, *11*, 472.

[21] H. Nakanishi, T. Yoshii, S. Kawasaki, K. Hayashi, K. Tsutsui, C. Oki, S. Tsukiji, H. Saito, *Cell Chem. Biol.* **2021**, *28*, 662–674.e665.
[22] H. Zhang, R. Zhao, J. Tones, M. Liu, R. L. Dilley, D. M. Chenoweth, R. A. Greenberg, M. A. Lampson, *Mol. Biol. Cell* **2020**, *31*, 2048–2056.
[23] X. Chen, M. Venkatachalapathy, D. Kamps, S. Weigel, R. Kumar, M. Orlich, R. Garrecht, M. Hirtz, C. M. Niemeyer, Y.-W. Wu, L. Dehmelt, *Angew. Chem. Int. Ed.* **2017**, *56*, 5916–5920; *Angew. Chem.* **2017**, *129*, 6010–6014.
[24] V. M. Krishnamurthy, V. Semetey, P. J. Bracher, N. Shen, G. M. Whitesides, *J. Am. Chem. Soc.* **2007**, *129*, 1312–1320.
[25] T. Tsuruo, H. Iida, S. Tsukagoshi, Y. Sakurai, *Cancer Res.* **1981**, *41*, 1967–1972.
[26] a) M. Pettersson, X. Hou, M. Kuhn, T. T. Wager, G. W. Kauffman, P. R. Verhoest, *J. Med. Chem.* **2016**, *59*, 5284–5296; b) B. E. Smart, *J. Fluorine Chem.* **2001**, *109*, 3–11.
[27] J. R. Appleman, N. Prendergast, T. J. Delcamp, J. H. Freisheim, R. L. Blakley, *J. Biol. Chem.* **1988**, *263*, 10304–10313.
[28] M. P. Krafft, J. G. Riess, *Biochimie* **1998**, *80*, 489–514.
[29] M. B. Stone, S. A. Shelby, S. L. Veatch, *Chem. Rev.* **2017**, *117*, 7457–7477.
[30] I. Manolaridis, K. Kulkarni, R. B. Dodd, S. Ogasawara, Z. Zhang, G. Bineva, N. O'Reilly, S. J. Hanrahan, A. J. Thompson, N. Cronin, S. Iwata, D. Barford, *Nature* **2013**, *504*, 301–305.
[31] B. Di Ventura, B. Kuhlman, *Curr. Opin. Chem. Biol.* **2016**, *34*, 62–71.
[32] T. Kanda, K. F. Sullivan, G. M. Wahl, *Curr. Biol.* **1998**, *8*, 377–385.
[33] a) Y. Shin, C. P. Brangwynne, *Science* **2017**, *357*, eaaf4382; b) S. Boeynaems, S. Alberti, N. L. Fawzi, T. Mittag, M. Polymenidou, F. Rousseau, J. Schymkowitz, J. Shorter, B. Wolozin, L. Van Den Bosch, P. Tompa, M. Fuxreiter, *Trends Cell Biol.* **2018**, *28*, 420–435.
[34] a) D. Hnisz, K. Shrinivas, R. A. Young, A. K. Chakraborty, P. A. Sharp, *Cell* **2017**, *169*, 13–23; b) A. Boija, I. A. Klein, B. R. Sabari, A. Dall'Agnese, E. L. Coffey, A. V. Zamudio, C. H. Li, K. Shrinivas, J. C. Manteiga, N. M. Hannett, B. J. Abraham, L. K. Afeyan, Y. E. Guo, J. K. Rimel, C. B. Fant, J. Schuijers, T. I. Lee, D. J. Taatjes, R. A. Young, *Cell* **2018**, *175*, 1842–1855.e1816.
[35] a) X. Su, J. A. Ditlev, E. Hui, W. Xing, S. Banjade, J. Okrut, D. S. King, J. Taunton, M. K. Rosen, R. D. Vale, *Science* **2016**, *352*, 595–599; b) L. B. Case, J. A. Ditlev, M. K. Rosen, *Annual Rev. Biophys.* **2019**, *48*, 465–494.
[36] a) J. A. Riback, C. D. Katanski, J. L. Kear-Scott, E. V. Pilipenko, A. E. Rojek, T. R. Sosnick, D. A. Drummond, *Cell* **2017**, *168*, 1028–1040.e1019; b) T. M. Franzmann, M. Jahnel, A. Pozniakovsky, J. Mahamid, A. S. Holehouse, E. Nüske, D. Richter, W. Baumeister, S. W. Grill, R. V. Pappu, A. A. Hyman, S. Alberti, *Science* **2018**, *359*, eaao5654.
[37] a) J. P. Taylor, R. H. Brown, D. W. Cleveland, *Nature* **2016**, *539*, 197–206; b) I. R. Mackenzie, A. M. Nicholson, M. Sarkar, J. Messing, M. D. Purice, C. Pottier, K. Annu, M. Baker, R. B. Perkerson, A. Kurti, B. J. Matchett, T. Mittag, J. Temirov, G.-Y. R. Hsiung, C. Krieger, M. E. Murray, M. Kato, J. D. Fryer, L. Petrucelli, L. Zinman, S. Weintraub, M. Mesulam, J. Keith, S. A. Zivkovic, V. Hirsch-Reinshagen, R. P. Roos, S. Züchner, N. R. Graff-Radford, R. C. Petersen, R. J. Caselli, Z. K. Wszolek, E. Finger, C. Lippa, D. Lacomis, H. Stewart, D. W. Dickson, H. J. Kim, E. Rogaeva, E. Bigio, K. B. Boylan, J. P. Taylor, R. Rademakers, *Neuron* **2017**, *95*, 808–816.e809; c) A. Molliex, J. Temirov, J. Lee, M. Coughlin, A. P. Kanagaraj, H. J. Kim, T. Mittag, J. P. Taylor, *Cell* **2015**, *163*, 123–133.
[38] W. Li, J. Hu, B. Shi, F. Palomba, M. A. Digman, E. Gratton, H. Jiang, *Nat. Cell Biol.* **2020**, *22*, 960–972.
[39] a) Y. Shin, J. Berry, N. Pannucci, M. P. Haataja, J. E. Toettcher, C. P. Brangwynne, *Cell* **2017**, *168*, 159–171.e114; b) Y. Shin, Y.-C. Chang, D. S. W. Lee, J. Berry, D. W. Sanders, P. Ronceray, N. S. Wingreen, M. Haataja, C. P. Brangwynne, *Cell* **2018**, *175*, 1481–1491.e1413; c) D. Bracha, M. T. Walls, M.-T. Wei, L. Zhu, M. Kurian, J. L. Avalos, J. E. Toettcher, C. P. Brangwynne, *Cell* **2018**, *175*, 1467–1480.e1413; d) E. Dine, A. A. Gil, G. Uribe, C. P. Brangwynne, J. E. Toettcher, *Cell Systems* **2018**, *6*, 655–663.e655; e) Y. Zhang, D. S. W. Lee, Y. Meir, C. P. Brangwynne, N. S. Wingreen, *Phys. Rev. Lett.* **2021**, *126*, 258102.
[40] A. R. Strom, C. P. Brangwynne, *J. Cell Sci.* **2019**, *132*, jcs235093.
[41] S. Elbaum-Garfinkle, Y. Kim, K. Szczepaniak, C. C.-H. Chen, C. R. Eckmann, S. Myong, C. P. Brangwynne, *Proc. Natl. Acad. Sci. USA* **2015**, *112*, 7189–7194.
[42] B. Wu, Y. Chen, J. D. Müller, *Biophys. J.* **2009**, *96*, 2391–2404.
[43] Q. Zhang, H. Huang, L. Zhang, R. Wu, C.-I. Chung, S.-Q. Zhang, J. Torra, A. Schepis, S. R. Coughlin, T. B. Kornberg, X. Shu, *Mol. Cell* **2018**, *69*, 334–346.e334.

Manuscript received: April 14, 2022
Revised manuscript received: May 18, 2022
Accepted manuscript online: May 22, 2022
Version of record online: ■■, ■■■

RESEARCH ARTICLE

Linkerology 101: This work presents a quantitative method for the rational design of tools to control protein-protein interactions. A library of probes based on the Trimethoprim-HaloTag system was synthesized and evaluated. The top-performing probe was used to control protein localization to various organelles within a cell and to initiate both local and global phase separation.

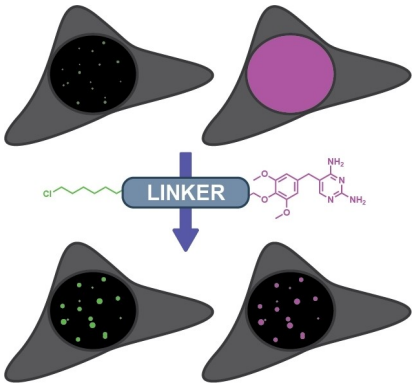

R. M. Lackner, W. O'Connell, Dr. H. Zhang, Dr. D. M. Chenoweth**